Family resemblances: A common fold for some dimeric ion-coupled secondary transporters

Ariela Vergara-Jaque,[1] Cristina Fenollar-Ferrer,[1] Christopher Mulligan,[2] Joseph A. Mindell,[2] and Lucy R. Forrest[1]

[1]Computational Structural Biology Unit and [2]Membrane Transport Biophysics Section, National Institutes of Neurological Disorders and Stroke, National Institutes of Health, Bethesda, MD 20824

Membrane transporter proteins catalyze the passage of a broad range of solutes across cell membranes, allowing the uptake and efflux of crucial compounds. Because of the difficulty of expressing, purifying, and crystallizing integral membrane proteins, relatively few transporter structures have been elucidated to date. Although every membrane transporter has unique characteristics, structural and mechanistic similarities between evolutionarily diverse transporters have been identified. Here, we compare two recently reported structures of membrane proteins that act as antimicrobial efflux pumps, namely MtrF from *Neisseria gonorrhoeae* and YdaH from *Alcanivorax borkumensis*, both with each other and with the previously published structure of a sodium-dependent dicarboxylate transporter from *Vibrio cholerae*, VcINDY. MtrF and YdaH belong to the *p*-aminobenzoyl-glutamate transporter (AbgT) family and have been reported as having architectures distinct from those of all other families of transporters. However, our comparative analysis reveals a similar structural arrangement in all three proteins, with highly conserved secondary structure elements. Despite their differences in biological function, the overall "design principle" of MtrF and YdaH appears to be almost identical to that of VcINDY, with a dimeric quaternary structure, helical hairpins, and clear boundaries between the transport and scaffold domains. This observation demonstrates once more that the same secondary transporter architecture can be exploited for multiple distinct transport modes, including cotransport and antiport. Based on our comparisons, we detected conserved motifs in the substrate-binding region and predict specific residues likely to be involved in cation or substrate binding. These findings should prove useful for the future characterization of the transport mechanisms of these families of secondary active transporters.

INTRODUCTION

Secondary active transporters transport a panoply of substrates against their electrochemical gradients by coupling their movement to the "downhill" transit of one or more small inorganic ions, most commonly H^+ or Na^+. Organisms across the living kingdoms use these proteins for a host of biological functions, from nutrient uptake to xenobiotic removal. Secondary active transporters have been classified in several ways, i.e., based on sequence similarity, substrate specificity, or structural fold (Prakash et al., 2003; Chen et al., 2011; Forrest et al., 2011). Our mechanistic understanding of these proteins has progressed far in the last decade, in large part because of the increasing number of atomic resolution x-ray crystal structures of such transporters. One unexpected revelation as a result of this development is the discovery that many transporters, previously thought to be unrelated, actually share common tertiary protein folds. For example, the structure of LeuT, a member of the neurotransmitter/sodium symporter family, was first solved by the Gouaux laboratory (Yamashita et al., 2005), after which a series of subsequent structures, including Mhp1 (Weyand et al., 2008), ApcT (Shaffer et al., 2009), BetP (Ressl et al., 2009), AdiC (Fang et al., 2009), vSGLT (Watanabe et al., 2010), GadC (Ma et al., 2012), MhsT (Malinauskaite et al., 2014), and ScaDMT (Ehrnstorfer et al., 2014), turned out to be structurally similar despite extremely limited sequence similarity. Comparisons of these proteins have led to insight into shared and divergent features of their mechanisms. In contrast, some other transporter structures have not followed this pattern. For example, the structural folds represented by the aspartate transporter Glt_{Ph} (Yernool et al., 2004), the nucleoside transporter VcCNT (Johnson et al., 2012), and the succinate transporter VcINDY (Mancusso et al., 2012) are so far unique and without parallel in other structures determined to date.

Two recent papers, published almost simultaneously, described new structures of proteins with reportedly unique folds. One of these proteins, MtrF from *Neisseria gonorrhoeae* (the causative agent of gonorrhea; Su et al.,

The Rockefeller University Press $30.00
J. Gen. Physiol. Vol. 146 No. 5   423–434
www.jgp.org/cgi/doi/10.1085/jgp.201511481

423

2015), is thought to be an antimicrobial efflux pump (Folster and Shafer, 2005; Su et al., 2015). The MtrF structure reveals a dimer, with nine transmembrane (TM) helices and two helical hairpins (HPs) in each protomer. Expression of MtrF in *Escherichia coli* conferred resistance to several sulfonamide antimicrobials and reduced the accumulation of radiolabeled sulfamethazine in the bacteria, consistent with the proposed role for MtrF in antimicrobial resistance. The other protein, YdaH from *Alcanivorax borkumensis* (Bolla et al., 2015), also reported as a unique fold, has remarkably similar features: dimeric structure, nine TM helices, and two hairpins per protomer. Moreover, YdaH also conferred sulfonamide resistance and reduced the accumulation of radiolabeled sulfa drugs in *E. coli* (Bolla et al., 2015). On visual inspection, these protein structures also look similar, perhaps unsurprisingly, as both belong to the *p*-aminobenzoyl-glutamate transporter AbgT gene family (transporter classification database [TCDB] 2.A.68; Saier et al., 2006; Su et al., 2015).

We were further surprised that, to our eyes, both of these protein structures also appear quite similar to a structure of the Na⁺-coupled succinate transporter VcINDY (Mancusso et al., 2012). VcINDY belongs to the divalent anion/Na⁺ symporter (DASS) family (TCDB 2.A.47) and is homologous to transporters in the human solute carrier family 13, SLC13 (Bergeron et al., 2013). It has been proposed, based on bioinformatic analysis, that the DASS and AbgT families are distant relatives belonging to a single superfamily called the ion transporter superfamily (Prakash et al., 2003; Chen et al., 2011). Here, we use computational methods to test the hypothesis that, like the LeuT family, these apparently unrelated structures share the same basic fold. We demonstrate that all three proteins share common structural features, confirming their assignment within the ion transporter superfamily (Prakash et al., 2003; Chen et al., 2011). MtrF, YdaH, and VcINDY also exhibit interesting sequence hallmarks that were reported previously for VcINDY (Mancusso et al., 2012), but not for YdaH and MtrF. These structural similarities suggest an underlying mechanistic unity across the superfamily. Here we take advantage of these structural similarities to predict binding sites for ions not resolved in some of the structures. The identification of subtle structural differences may yield insight into the adaptations necessary to bind strikingly different substrates.

MATERIALS AND METHODS

Structural comparison

A structural comparison of the transporters VcINDY (Protein Data Bank [PDB] accession no. 4F35; Berman et al., 2000; Mancusso et al., 2012), MtrF (PDB accession no. 4R1I; Su et al., 2015), and YdaH (PDB accession no. 4R0C; Bolla et al., 2015) was performed using the fragment-based structure alignment program Fr-TM-align (Pandit and Skolnick, 2008), which is one of the most accurate methods for structurally aligning membrane proteins (Stamm and Forrest, 2015). Several alignments were performed; in each case, we compared all combinations of the three structures, namely MtrF aligned with VcINDY, YdaH aligned with VcINDY, and MtrF aligned with YdaH. Individual protomers in the dimer were compared using chain A of each PDB file. Each protomer was also divided into two segments, using definitions similar to that of the sodium-coupled aspartate transporter Glt$_{Ph}$ (Reyes et al., 2009). In Glt$_{Ph}$, the substrate is bound within a discreet domain called the transport domain, which moves independently of the helices at the oligomer interface (Reyes et al., 2009). The helices that encompass the substrate-binding site, and that appear likely to move during the conformational change, were defined as the transport domain. This segment is equivalent to the so-called outer core region defined for MtrF (Su et al., 2015). The helices contributing to the dimer interface in VcINDY, MtrF, and YdaH (the oligomerization domain) were treated as part of a larger, so-called scaffold domain, including helices that link to the transport domain. This designation is equivalent to the inner core of MtrF (Su et al., 2015). The scaffold and transport domains of each structure were also compared separately. In VcINDY, the scaffold and transport domains were defined as residues 19–126 plus 253–356, and residues 127–242 plus 357–462, respectively. In MtrF, residues 10–126 and 253–391 define the scaffold domain, whereas the transport domain was defined as residues 127–252 and 392–516. In YdaH, the scaffold and transport domains were defined as residues 17–113 plus 244–372, and residues 114–243 plus 373–492, respectively. The position of VcINDY and MtrF in the membrane was determined with the Orientations of Proteins in Membranes (OPM) server (Lomize et al., 2006), and the orientation of YdaH was defined after superposition of the YdaH dimer onto that of MtrF. Sequence alignments were reported by Fr-TM-align and reflect the residues closest in space after structural alignment. Secondary structure assignments were estimated for the x-ray structures using the Define Secondary Structure of Proteins (DSSP) program (Kabsch and Sander, 1983). Alignments were rendered with the Jalview (version 2.8) software (Waterhouse et al., 2009).

Binding pocket analysis

The surface of the binding pocket in each structure was calculated using the CAVER 3.0.1 program (Petřek et al., 2006) with default parameters. The starting point for the calculation of the volume was the center of mass of the Cα atoms of residues 150–152, 377–379, and 421 in VcINDY; for MtrF and YdaH, the transport domains were first superimposed onto that of VcINDY before computing the volume. For analysis of the sodium sites, the structures of YdaH and MrtF, as well as the model of human NaPi-IIa previously reported by Fenollar-Ferrer et al. (2014), were superimposed onto the structure of VcINDY. Putative binding site residues (Ser, Thr, Asn, Gln, Asp, or Glu) were identified within 8 Å of any of the sodium ions (Na2 in VcINDY or Na3 in YdaH) after superimposition. All figures were generated using PyMOL (version 1.6; Schrödinger, LLC). Helix–helix packing angles were calculated using PyMOL.

Sequence analysis

Sequence homologues of the three proteins were identified using Jackhmmer (Finn et al., 2011), with one iteration, against the "55 representative proteomes" sequence database. The obtained sequences were sorted by length and clustered at 90% identity using the UCLUST algorithm (version 1.2; Edgar, 2010). Short sequences, that is, <450 or <350 amino acids long, for VcINDY or MtrF/YdaH, respectively, were excluded, leaving 414, 187, and 176 homologues of VcINDY, MtrF, and YdaH, respectively. Multiple-sequence alignments were then built with the MAFFT server (Katoh and Standley, 2013) and analyzed with Jalview (Waterhouse

et al., 2009). The conservation of residues was estimated as residue probabilities using the Weblogo server (version 3.4; Crooks et al., 2004).

RESULTS

A similar structural arrangement

Visual inspection of VcINDY, MtrF, and YdaH suggests a similar three-dimensional fold and topology. VcINDY is dimeric, with each protomer containing 11 TM α helices. MtrF and YdaH are also dimers, but with nine α-helical TM segments in each subunit. As shown in Fig. 1, the spatial distribution of the subdomains in the three transporters is almost identical, with helices at the central oligomerization interface (dark blue) combined with additional peripheral helices (cyan) together providing a scaffold (scaffold domain) that frames the core substrate-binding, or transport, domain (green; see Materials and methods).

Notwithstanding the fact that the VcINDY structure has two additional TM helices, all three proteins carry several conserved structural elements (Fig. 1). Within the scaffold domain, the tripartite helices TM4 and TM9 of VcINDY correspond to TM2 and TM7 of MtrF and YdaH, while in the transport domain, the interrupted helices TM5 and TM10 of VcINDY are equivalent to TM3 and TM8 of MtrF and YdaH. The TM topologies of the transport domains are identical in all three structures, including the presence of two HPs. Each HP enters and exits the membrane on the same side, and these motifs are therefore also known as reentrant helices. HPs proximal to a canonical helix as well as to an
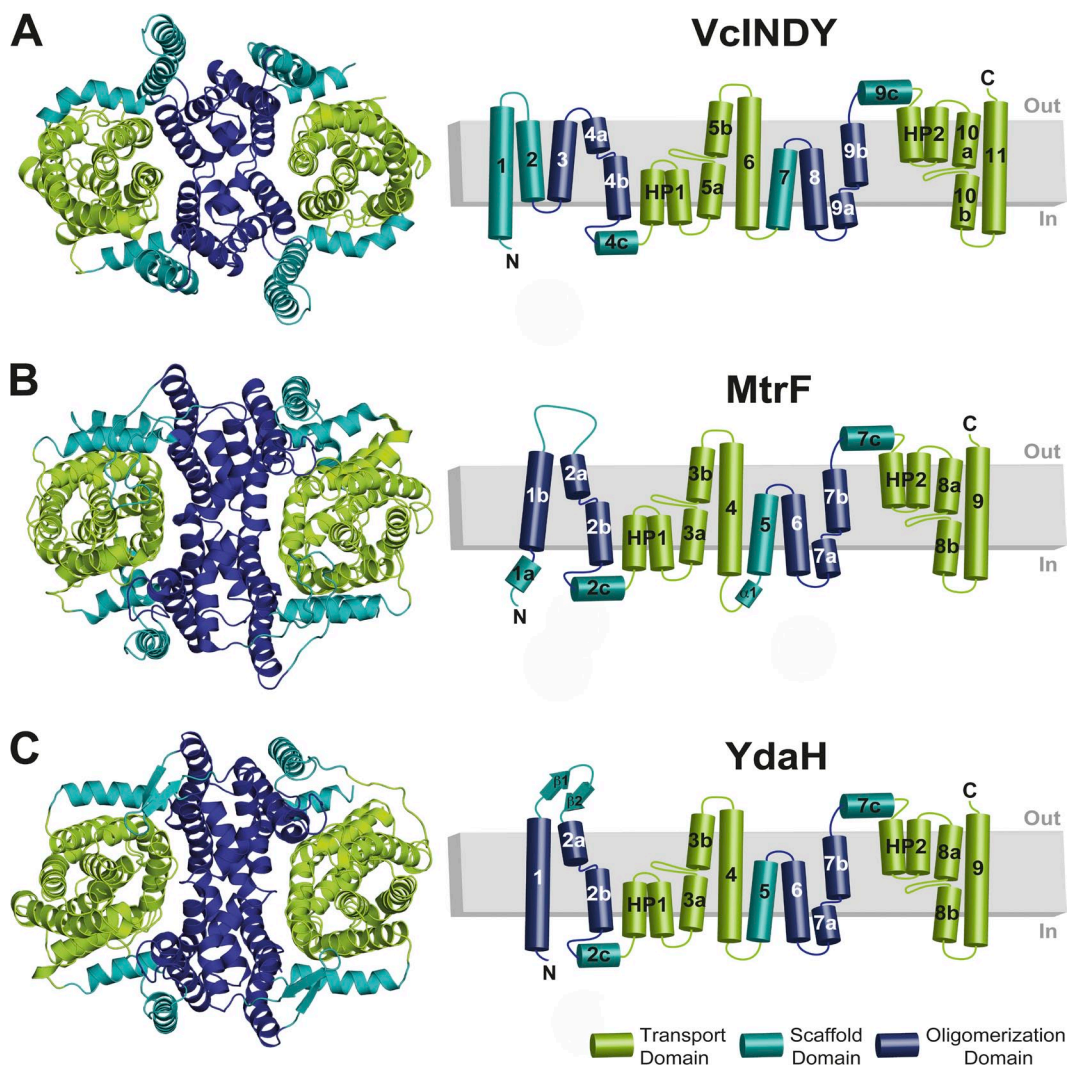

Figure 1. Structure of the VcINDY, MtrF, and YdaH transporters. Cartoon representation of the VcINDY (A), MtrF (B), and YdaH (C) dimer structures shown from the extracellular side of the membrane (left). The scaffold domain is colored cyan and dark blue, with the dark blue regions indicating helices involved in oligomerization. The transport domain containing the substrate-binding site(s) is colored green. The helices forming each domain are detailed in the topology diagrams to the right. HPs 1 and 2 correspond to HPin and HPout, respectively, in the nomenclature of Mancusso et al. (2012).

interrupted helix with an intramembrane loop have mechanistic roles in other membrane-transport proteins of known structure, namely Glt$_{Ph}$ (Yernool et al., 2004) and the concentrative nucleoside transporter from *Vibrio cholerae*, VcCNT (Johnson et al., 2012).

The most significant difference between the three proteins is found in the N-terminal region, where TM1, TM2, and TM3 of VcINDY are reduced to a single TM helix, TM1 in MtrF and YdaH. In addition, although the MtrF and YdaH structures seem to be quite similar, there are subtle differences: TM1 is interrupted in MtrF, the TM1–TM2 loop forms a β hairpin in YdaH, and the TM4–TM5 loop contains a short helix (α1) only in MtrF.

Importantly, in all three proteins, the N-terminal half of the protein relates to the C-terminal half by a twofold pseudo-symmetry, with the two halves oriented in opposite directions and the symmetry axis parallel to the membrane plane. These two structural repeats in VcINDY are formed by TM2–TM6 and TM7–TM11, whereas the repeats in MtrF and YdaH comprise helices TM1–TM4 and TM6–TM9. Although rare among membrane proteins in general, inverted-topology pseudo–C2 symmetry is common to around three fourths of secondary transporter folds (Forrest, 2015), and appears to facilitate a conformational mechanism of alternating access involving asymmetry exchange (Forrest et al., 2008; Crisman et al., 2009; Forrest, 2015).

Structurally equivalent segments

As a quantitative assessment of the differences between VcINDY, MtrF, and YdaH, we performed a structural comparison of the protomers after alignment with FR-TM-align (Fig. 2; Pandit and Skolnick, 2008). The MtrF and YdaH structures are extremely similar, with a root mean square deviation (RMSD) of the Cα atoms of 2.1 Å. The structural alignment between the protomers of MtrF and VcINDY yields a somewhat lower RMSD of 4.3 Å, whereas the RMSD between YdaH and VcINDY was 4.6 Å. We also compared the structural similarity using the so-called template modeling score (TM-score), a normalized length-independent measure, where a TM-score >0.5 indicates that two structures have essentially the same fold (Zhang and Skolnick, 2004). The TM-scores of the MtrF-VcINDY, YdaH-VcINDY, and MtrF-YdaH alignments were 0.72, 0.72, and 0.94, respectively. Thus, the structures of MtrF and YdaH are clearly more similar to each other than either structure is to that of VcINDY.

Comparing only the scaffold domains (defined hereafter as including the helices in the oligomerization interface), the RMSD between MtrF and VcINDY was 4.7 Å, whereas for the YdaH-VcINDY alignment, the RMSD was 5.1 Å. In both cases, the TM-score for these local evaluations was 0.55, consistent with weak fold similarity. In contrast, the scaffold domains in MtrF-YdaH are clearly more closely conserved, with an RMSD of 1.9 Å and a TM-score of 0.90. Fig. 2 B illustrates the major

structural differences between VcINDY and the other two proteins (red). Some of these differences, such as the presence of a short helix α1 in MtrF, were noted in the topology comparison above. Other differences may arise as a result of the low confidence of the loop structures, especially for the peripheral regions of MtrF, such as the TM1–TM2 loop, which have the lowest resolution and the highest temperature factors (not depicted). Interestingly, TM1 of MtrF and YdaH contributes to the dimer interface, whereas TM1 in VcINDY does not. We also note the possibility that TM2 and TM3 of VcINDY evolved from, or into, the two antiparallel β strands in YdaH, and into the long unstructured TM1–TM2 loop in MtrF.

For the transport domains, the three structural alignments (Fig. 2 C) revealed a high structural homology. For the MtrF-VcINDY, YdaH-VcINDY, and MtrF-YdaH alignments, the RMSD values were 3.3, 2.9, and 1.8 Å, and the TM-scores were 0.74, 0.77, and 0.92, respectively. The most important differences in the transport domain were found in the TM3b and TM8b helices of MtrF and YdaH, which are equivalent to TM5b and TM10b, respectively, in VcINDY. These helices have different lengths and orientations in the three transporters, as described in detail below.

Conformational and substrate-bound states

Visual inspection of the crystal structures of VcINDY, MtrF, and YdaH reveals a similar conformational state of the protomers in the membrane, with all three proteins adopting conformations in which the presumed substrate-binding sites face the cytoplasm (Fig. 3, A–C).

The binding sites in the three transporter structures include different substrates, reflecting their different specificities and/or differences in crystallization conditions. The F_o–F_c map of VcINDY contains positive densities that were assigned to a citrate molecule and a sodium ion in each protomer, whereas YdaH has density assigned to one sodium ion per protomer. However, there was no evidence for a bound substrate in the structure of MtrF, either because the structure represents an apo state or because the resolution of the structure (3.95 Å) is too low to resolve the substrate.

Comparison of the transport domains revealed similar folds and orientations for HP1 and HP2, TM4 or TM6 (in YdaH/MtrF or VcINDY, respectively), as well as for TM9 or TM11 (Fig. 3, A–C, right). However, the interrupted helices TM3 or TM5 and TM8 or TM10 show important differences between the three protein structures. Specifically, in MtrF and YdaH, TM3b and TM8b are longer than the equivalent helices TM5b and TM10b in VcINDY. Moreover, the angle of TM3b relative to HP2b increases by ∼21° in YdaH relative to VcINDY, and by a further ∼6° in MtrF (Fig. 3 D). This difference in helix orientation is potentially correlated with substrate or inhibitor binding, as the binding pocket appears

to be smallest in the structure of VcINDY with citrate and sodium bound (Fig. 3, A–C, right). Thus, TM3b may provide a "lid" over the substrate-binding site, which will be tilted in the substrate-free conformation and more straight in the "closed," substrate-occluded state, analogous to the lid formed by HP2 in Glt$_{Ph}$ (Boudker et al., 2007). However, it is also possible that the differences between the binding sites in the three structures reflect their different sequences and substrate specificities rather than changes between apo and holo states.
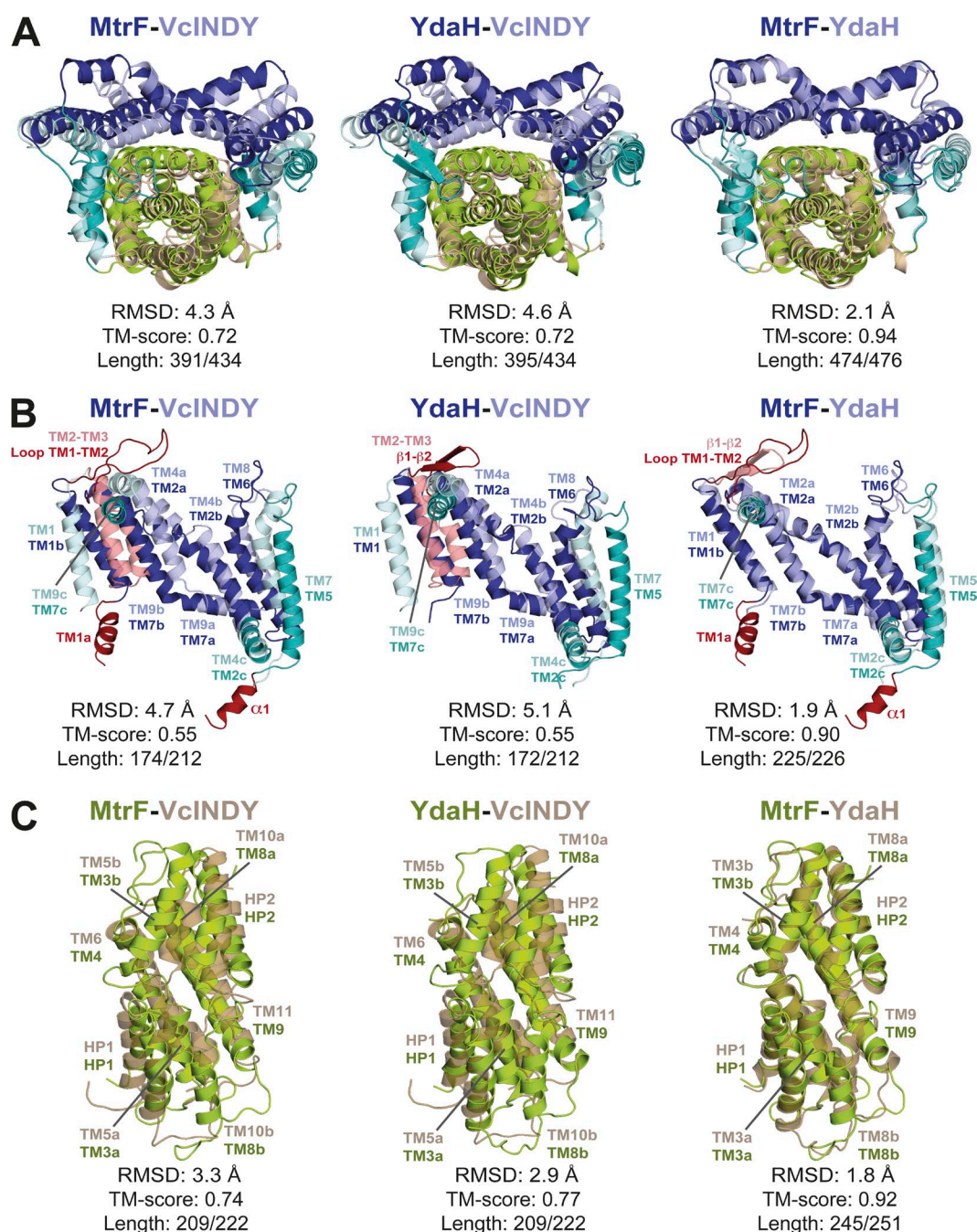

Figure 2. Structural comparison of the VcINDY, MtrF, and YdaH transporters. (A) A structural alignment of the whole structure of each protomer is shown from the extracellular side of the membrane, with the helices colored according to the topology. The MtrF-VcINDY, YdaH-VcINDY, and MtrF-YdaH alignments are shown on the left, middle, and right, respectively. The structural superimpositions of the scaffold-oligomerization (B) and transport (C) domain are shown from a view parallel to the membrane plane. The scaffold-oligomerization domains exhibit the most significant differences, which are highlighted in red. The structural alignments were obtained using the program Fr-TM-align. The RMSD and TM-score of the structural alignment are given in each case, along with the number of aligned residues and the length of the shortest input.
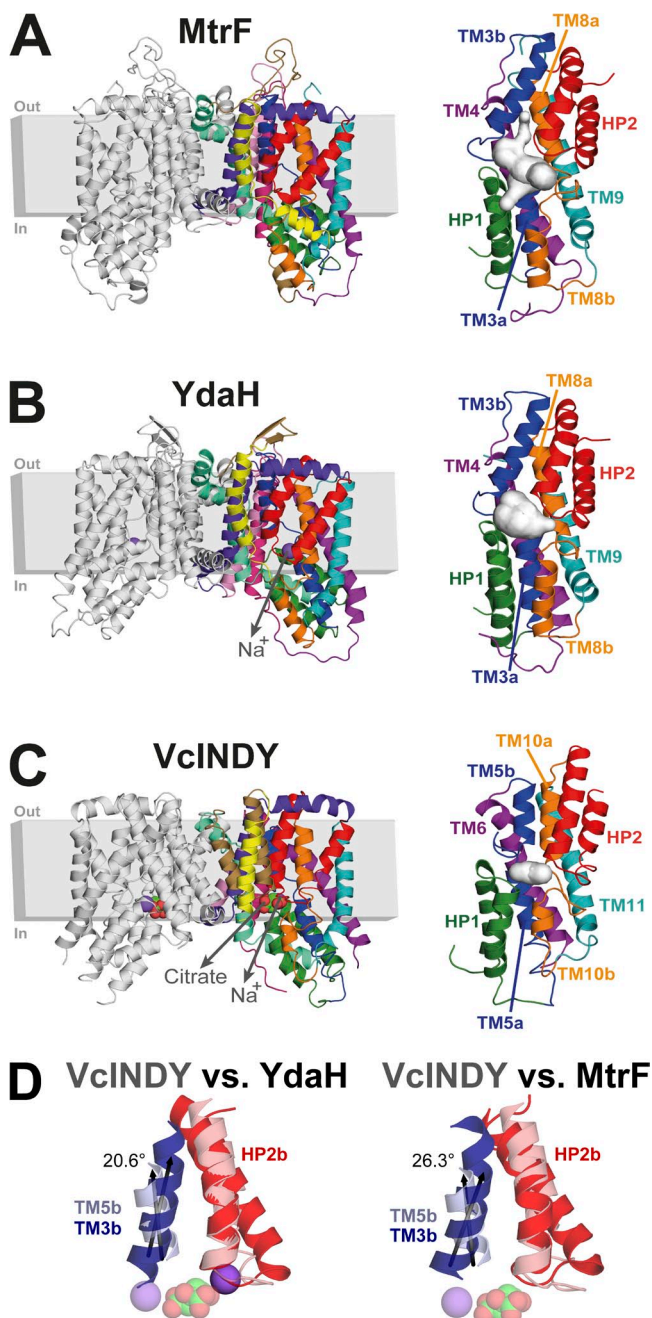
Conserved motifs in the binding sites

The functional data reported so far for the three transporters suggest differences in the type of coupling ion. Specifically, VcINDY is a sodium-dependent dicarboxylate transporter (Mulligan et al., 2014), whereas MtrF was proposed to be a proton-motive force (PMF)-dependent efflux pump (Su et al., 2015), and YdaH is a PMF-dependent *p*-aminobenzoyl-glutamate transporter also regulated by sodium (Bolla et al., 2015). Notably, VcINDY is a cotransporter, whereas the evidence for MtrF and YdaH suggests that they both function as antiporters. In spite of these differences in function, the three transporters share important amino acid motifs in their binding sites.

Overall, the sequence alignments extracted from structural superposition of MtrF-VcINDY, YdaH-VcINDY, and MtrF-YdaH reveal 11.2, 15.5, and 44.1% identical residues and 34.0, 36.5, and 63.7% similar residues, respectively (Fig. 4). Focusing on the tips of the HPs reveals interesting sequence motifs, close to the substrate-binding sites, which have been described previously only for transporters of the DASS family (Mancusso et al., 2012). In the loop connecting HP1a and HP1b, homologues of all three proteins contain an S[NHS]xA[ST] motif (Fig. 5, left). In YdaH and MtrF, this motif is followed by a conserved acidic residue (asp or glu). HP2 contains a similar motif (Fig. 5, right). In VcINDY homologues, this sequence is typically S[NH]T[AV][TAS], whereas in MtrF and YdaH homologues, the motif is S[AG]SAΦ, where Φ is usually large and polar (lys or asn).

We note that neither the HP1 motif nor the HP2 motif is 100% conserved. For example, HP1 in YdaH contains the sequence SSLTVD; that is, the last Ser/Thr residue has been replaced by Val relative to MtrF and VcINDY. In addition, the HP1 motif is located in slightly different positions in the structure: either within HP1b in VcINDY or closer to HP1a in MtrF and YdaH (see Fig. 4). Nevertheless, the fact that a similar pattern is found in both the DASS and AbgT families, which have very diverse sequences overall, suggests that these regions are important for function and may be involved in cation binding or play a structural role.

Site-directed mutagenesis of the second serine in the HP2 motif to alanine in MtrF (S417A) reduced the ability of *E. coli* cells to accumulate sulfamethazine (Su et al., 2015), supporting our proposal that this residue is an important component of a functional motif. To analyze these motifs and other residues involved in cation

Figure 3. Ligand pathways and binding sites in the three inward-facing structures. Cartoon representation of the MtrF (A), YdaH (B), and VcINDY (C) dimer structures viewed along the membrane plane. The subunits on the right are colored with separate colors for each helix. Ligands are shown as spheres, with their presumed pathways illustrated using arrows. The position of the dimers in the membrane was determined for the x-ray structures using the Orientations of Proteins in Membranes (OPM) server. Each of the three transporters forms an upside-down bowl-shaped structure with a concave aqueous basin facing the intracellular side. VcINDY has a citrate molecule and a Na⁺ ion modeled in the binding site of each protomer, whereas YdaH has a Na⁺ ion in each protomer. No substrate was detected in the MtrF structure. To the right of each dimer, the transport domain is shown with a surface representation of the binding pocket in white, indicating that the binding sites vary in size in the presence of substrates. (D) Comparison of the tilt angle of TM5b in VcINDY (light blue and pink) with either TM3b of YdaH (left; dark blue and red) or TM3b of MtrF (right; dark blue and red). The binding pockets were superimposed using the first three helix turns of HP2b, and the angle of TM3b relative to TM5b was calculated. The position of the ligands is shown for VcINDY (transparent spheres) and YdaH (purple sphere).

binding, we carried out a structural characterization of the known binding sites.

Sodium-binding sites

The structures of the VcINDY, MtrF, and YdaH dimers were determined at a resolution of 3.20, 3.95, and 2.96 Å, respectively (Mancusso et al., 2012; Bolla et al., 2015; Su et al., 2015). Thanks to their higher resolution, the most reliable binding site details can be obtained from the structures of YdaH and VcINDY. The crystallographic analysis of VcINDY revealed a positive peak in the F_o–F_c map that was assigned to a sodium ion at a position between HP1 and the unwound segments of TM5 (Mancusso et al., 2012). For reasons that will become clear, we refer to this site as "Na2," consistent with previous work on the sodium phosphate cotransporter NaPi-IIa
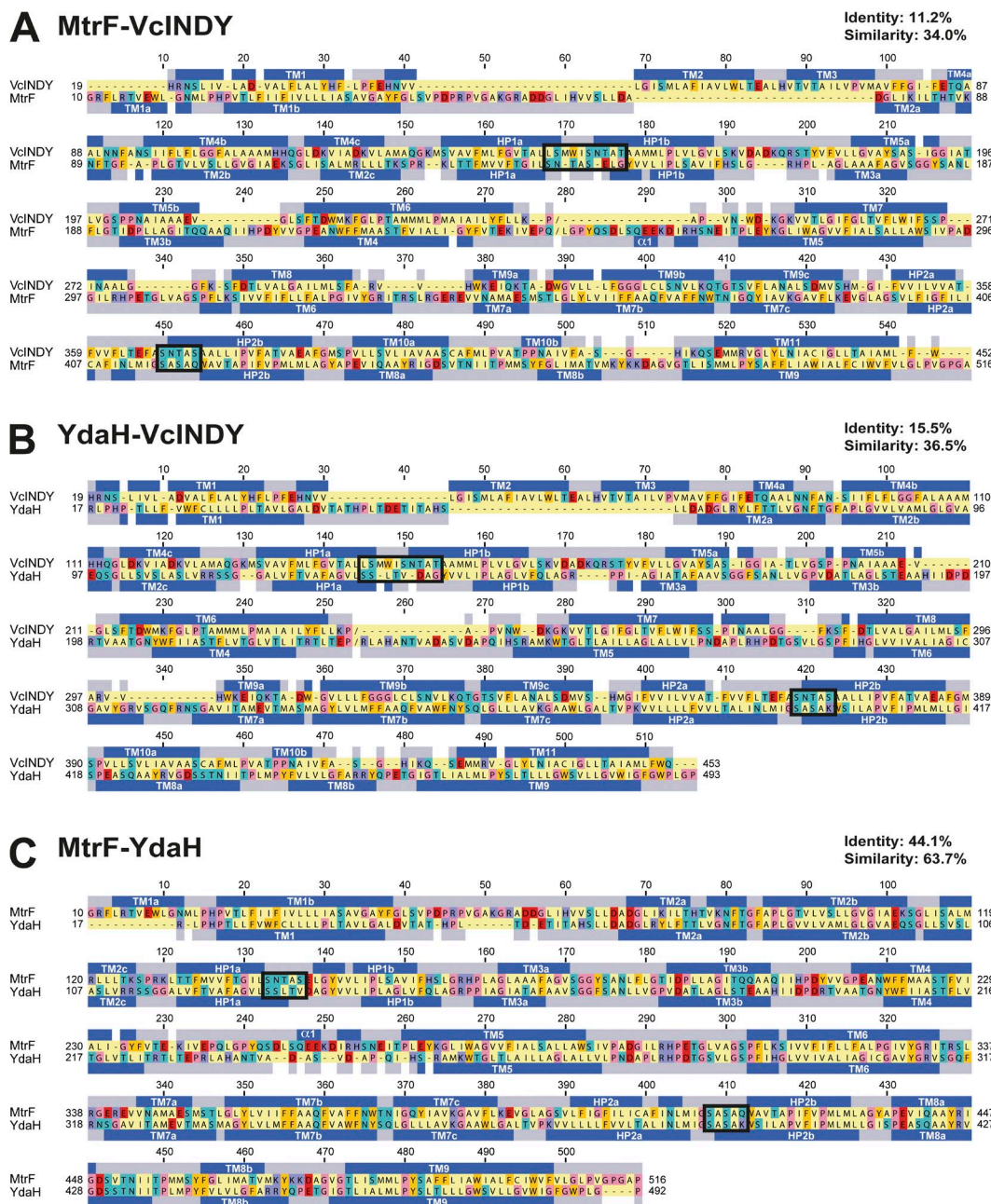

Figure 4. Sequence analysis of the three transporters. Sequence alignment between MtrF and VcINDY (A), YdaH and VcINDY (B), and MtrF and YdaH (C), extracted from the structure alignment obtained with the Fr-TM-align program. The sequence identity and similarity are given in each case. The alignment is colored according to the chemical properties of the residues: pale yellow, aliphatic (Ala, Ile, Leu, Met, and Val) and cysteine; cyan, polar uncharged (Asn, Gln, Ser, and Thr); yellow-orange, aromatic (Phe, Trp, and Tyr); red, acidic (Asp and Glu); purple, basic (Lys, Arg, and His); pink, Gly and Pro. The secondary structure (helix) assignments were obtained with DSSP and are indicated by blue rectangles. Black rectangles mark the motifs involved in the substrate-binding sites.

(see below), rather than "Na1," as named by Mancusso et al. (2012). This Na2 site in VcINDY includes coordination from residues Ser146, Ser150, Asn151 (HP1), and Gly199 (in the loop between TM5a and TM5b, L5ab; Fig. 6 A). Two of these four residues, Ser150 and Asn151, belong to the HP1 motif, and all the residues in the Na2 site originate from the first structural repeat.

The structure of YdaH also revealed a density for a sodium ion, but in this case the site is located between HP2 and the broken helix TM8, that is, in the second repeat (Fig. 6 B). We refer to this position as the "Na3" site, and its coordination in YdaH involves side chains from residues Asn390, Asp429, and Asn433, as well as backbone atoms from Gly394 and Asp429. Interestingly, the two known sodium sites are in pseudo-symmetric positions in the overall fold, with Na2 within the first structural repeat (in VcINDY) and Na3 formed by the second repeat (but in YdaH). Each site is formed by the hairpin and the interrupted helix in its respective repeat. For VcINDY, a second sodium site was previously proposed based on internal pseudo-symmetry with the known site (Mancusso et al., 2012), and the current observations lend weight to that prediction. However, the VcINDY-Na2 and YdaH-Na3 sites are not ideally symmetric, presumably because of local differences in the sequence motifs. For example, the VcINDY site involves a conserved Asn residue at the N-terminal end of the second helix in HP1 (HP1b; Fig. 5 A), whereas the YdaH site involves a conserved Asn at the C-terminal end of the first helix of HP2 (HP2a; Fig. 5 C).

Recently, a sodium phosphate cotransporter, NaPi-II, was shown to have a similar fold to that of VcINDY, based on bioinformatic analysis combined with biochemical and electrophysiological studies (Fenollar-Ferrer et al., 2014). NaPi-II transports three sodium ions along with its substrate phosphate, and it is known that one sodium (Na1) binds in the absence of phosphate, whereas the other ions (Na2 and Na3) bind concurrently with phosphate (Forster et al., 1998, 2012; Forster, I.C. 2007. Workshop 5: The kidney: Cellular, tubular and vascular physiology, OSU: Mathematical Biosciences Institute). In the recent bioinformatic study, a homology model of NaPi-II was built using VcINDY as a template, and a binding site for a sodium ion (Na2) equivalent to that of VcINDY was proposed (Fenollar-Ferrer et al., 2014). This Na2 site in NaPi-II is formed primarily by residues from the first structural repeat (Fig. 6 D), as in VcINDY (Fig. 6 A). An additional site for a sodium ion in NaPi-II was predicted at the pseudo-symmetric position to the Na2 site, and therefore this putative Na3 site involves residues from the second repeat (Fig. 6 D). Mutation of the residues contributing to the predicted Na2 and Na3 sites in human NaPi-IIa (Gln417, Ser418, and Ser419 in HP2, and Thr451 and Thr454 in TM5; Fig. 6 D) abolished transport, although the mutants retained their ability to bind the first sodium (Na1), consistent with the predicted roles of these residues only in Na2 and Na3 binding (Fenollar-Ferrer et al., 2014). The predicted Na3 site in the NaPi-II model is in excellent agreement with the position of the Na3 site in the recent structure of YdaH (Fig. 6 D; compare Fig. 6 B). Specifically, the ion at Na3 and the Cα atoms of residues Ser418 and Thr454 in NaPi-IIa are <2 Å from the ion and the equivalent atoms in Gly394 and Asn433 in YdaH, validating the earlier NaPi-IIa model and providing support for the assignment of the YdaH density as a sodium ion.
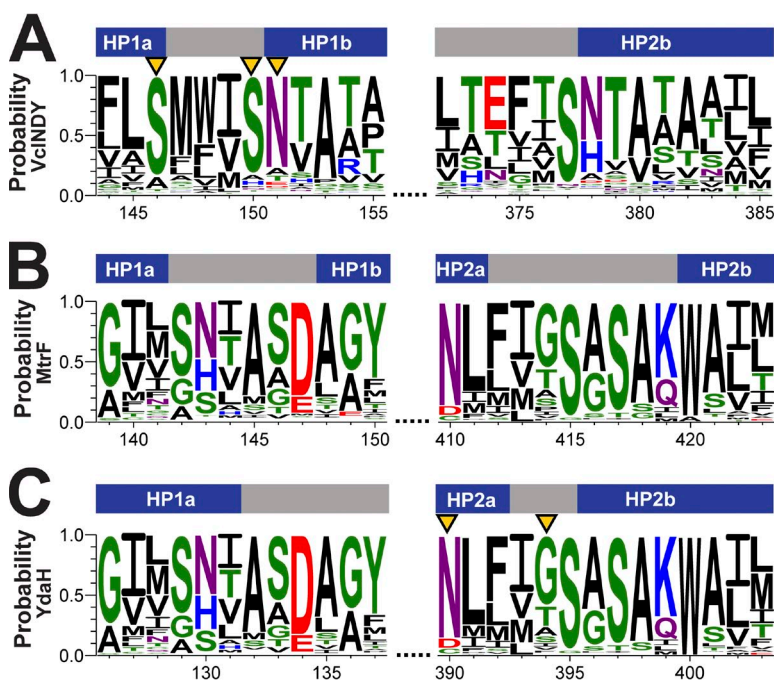

Figure 5. Sequence logos for key motifs in homologues of VcINDY, MtrF, and YdaH. The conservation of motifs for VcINDY (A), MtrF (B), and YdaH (C) was evaluated separately over a set of close homologues of each protein (≥90% identity). The motifs for YdaH are identical to that of MtrF because the set of homologues contain >90% of the same sequences. Multiple sequence alignments of the homologue sequences were built in each case, and logos were created with WebLogo (version 3.4; Crooks et al., 2004). The secondary structure assignments are indicated by blue (helix) and gray (loop) rectangles. Yellow triangles indicate the residues involved in sodium binding according to the structural data.

Putative sodium-binding sites

Although only a single Na^+ ion site was identified in VcINDY, succinate symport requires at least three Na^+ ions (Mulligan et al., 2014). Thus, additional sites must be present elsewhere in the VcINDY structure; these ions are not detected presumably either because of the low (3.2-Å) resolution or because of the particular conformational state of the protein in the crystal. For YdaH, on the other hand, the sodium/substrate stoichiometry is not known (Bolla et al., 2015). Here, we compare the structures of the two transporters to predict Na^+-binding sites in VcINDY, and to examine whether and/or where YdaH might bind a second cation. Specifically, after superposition of YdaH onto VcINDY, we identified all polar and acidic residues with side chains within 8 Å of either of the crystallographic sodium ions (Na2 in VcINDY or Na3 in YdaH; Fig. 6, A and B).

Residues fulfilling these criteria in VcINDY (in the region equivalent to Na3 in YdaH) include: Thr373, Ser377, Asn378, Thr379, and Ser381 in HP2; and Ser412 and Thr421 in the loop between TM10a and TM10b, L10ab (Fig. 6 A). Notably, the five residues from HP2 belong to the sequence TxxxSNTxT in the second repeat of VcINDY, and are therefore equivalent to the residues in the HP1 motif that form the Na2 site (Fig. 5 A). Indirect support for a role for several of these residues (Ser377, Asn378, Ser412, and Thr421) is provided by the deleterious effects of mutations of the corresponding
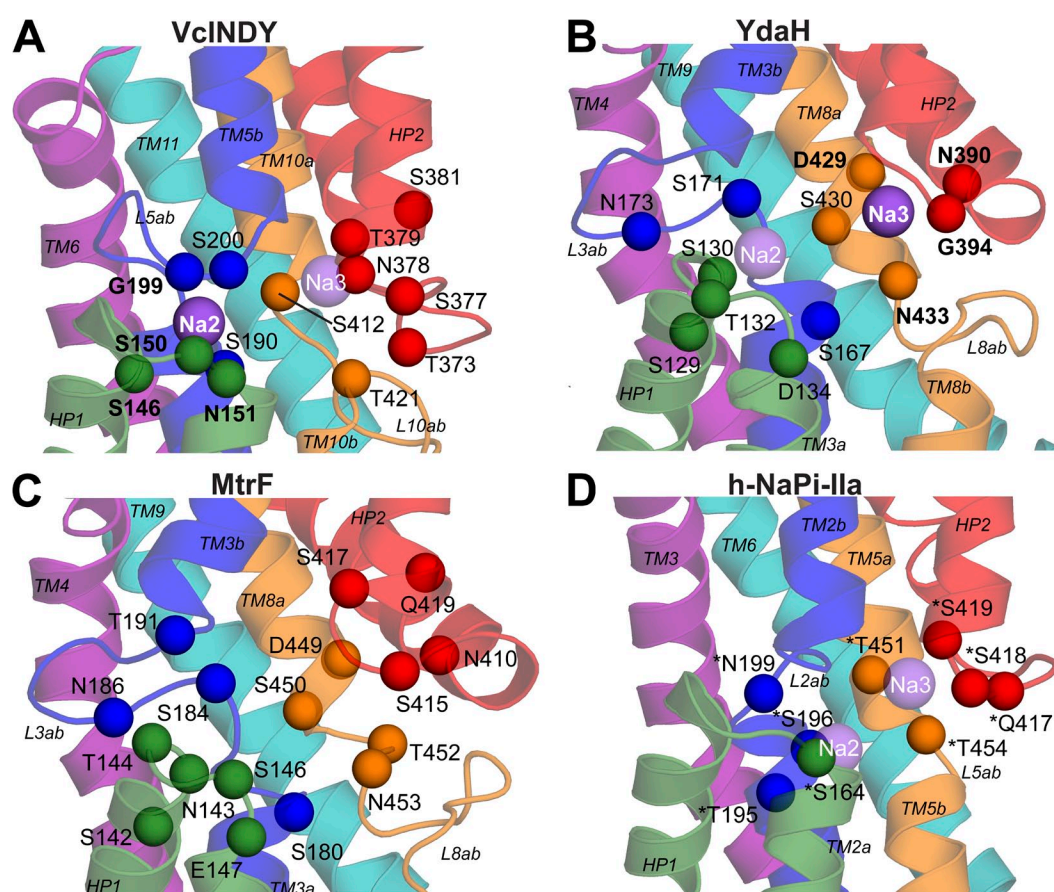

Figure 6. Known and predicted binding ion sites in the ion transporter superfamily fold. Two Na^+-binding sites have been reported based on the experimental electron density; these ions are shown as opaque purple spheres, and residues coordinating those ions directly are indicated by labels in bold font. (A) In VcINDY (PDB accession no. 4F35), a density was identified at the region labeled Na2. (B) In YdaH (PDB accession no. 4R0C), a density was identified at the region labeled Na3. The corresponding sites in VcINDY (Na3) and YdaH (Na2), shown as transparent spheres, were predicted after superposing YdaH on VcINDY with Fr-TM-align. Putative coordinating residues (Asn, Gln, Asp, Glu, Thr, or Ser within 8 Å of the ion) for the predicted YdaH-Na2 and VcINDY-Na3 site regions are indicated with spheres and labeled. The ion nomenclature follows that adopted previously for NaPi-II (see Results). The protein is shown as ribbons, and residues of interest are highlighted using spheres at the position of the Cα atom. (C) The equivalent region in MtrF (PDB accession no. 4R1I), which is a putative H^+-coupled transporter. (D) Structural model of human NaPi-IIa, with ions placed according to the results from VcINDY and YdaH shown as purple spheres. For NaPi-IIa, biochemical and electrophysiological evidence supports a role in phosphate or sodium binding for the residues shown as spheres (*). During the transport cycle of NaPi-IIa, an additional sodium binds before Na2 and Na3, at a site named Na1 (not depicted). The structures of VcINDY, YdaH, and MtrF are oriented with the extracellular side toward the top of the page, whereas NaPi-IIa is oriented with the cytoplasmic side toward the top of the page, because it inserts in the membrane in the opposite direction from the other transporters.

residues in the Na3 site in NaPi-IIa (Fig. 6 D; Fenollar-Ferrer et al., 2014). These predictions for the Na3 site of VcINDY are broadly similar to those made previously based on internal symmetry (Mancusso et al., 2012), but the present analysis provides stronger support for the involvement of specific residues.

In the case of YdaH, the positions equivalent to the Na2 site of VcINDY that potentially also coordinate sodium in YdaH are residues Ser129, Ser130, Thr132, and Asp134 in HP1, and Ser167, Ser171, and Asn173 in TM3b in the loop between TM3a and TM3b, L3ab. The strong cation-binding character of these residues suggests that they might bind a sodium ion (Fig. 6 B), assuming a stoichiometry of two or more sodium ions. However, these residues could also be required for proton or substrate binding, or for some other aspect of function.

Finally, we also superimposed the structure of MtrF onto VcINDY and YdaH, and identified equivalent residues in MtrF within 8 Å of the two structurally determined ions (Fig. 6 C). This comparison identifies Glu147 in repeat 1 and Asp449 in repeat 2 as particularly notable residues close to the sodium-binding sites of VcINDY and YdaH. Because MtrF is dependent on the PMF and not on sodium, these acidic residues may become protonated during transport. More detailed predictions for MtrF are precluded by the low (3.95-Å) resolution of the MtrF structure and by the need for additional information about the coupling mechanism. Further analysis will be required to confirm the ion dependence, stoichiometry, and binding-site residues in YdaH, MtrF, and VcINDY.

DISCUSSION

In this study, we showed that three recently published x-ray crystallographic structures, which were reported as novel structural folds, are in fact related. The structures of two proteins from the AbgT family, YdaH and MtrF, are very similar, with only minor differences in peripheral loops, and an overall TM-score of 0.94, consistent with a sequence identity of 44%. These two structures also show common features with a previously reported structure of a sodium-coupled succinate symporter, VcINDY, which is from the family of DASS transporters. In particular, their TM topologies, the general architecture comprising oligomerization and transport domains, and the presence of hairpins and discontinuous helices within the transport domains are similar. Differences were detected in the number of TM helices, and their arrangement in the oligomerization domain, and these differences are likely to be robust despite the limited resolution of the three structures (ranging from 2.96 to 3.95 Å).

This analysis provides strong support for earlier bioinformatic analysis, suggesting that the DASS (TCDB 2.A.47) and AbgT (TCDB 2.A.68) families belong to a common superfamily, which was named the ion-transporter superfamily (Prakash et al., 2003; Chen et al., 2011). The observation that VcINDY and its homologues confer symport, whereas the AbgT transporters appear to conduct antiport, provides yet one more demonstration that the same secondary transporter architecture can be responsible for a plethora of distinct transport modes. The reasons why this particular fold was enlisted for these functional requirements remain unclear.

Our analysis and comparison of the few observed substrate/ion-binding sites in the three transporter structures provide several useful testable hypotheses for identification of the remaining uncharacterized sites. Specifically, we predict that for VcINDY, residues Thr373, Ser377, Asn378, Thr379, and Ser381 in HP2, and Ser412 and Thr421 in the L10ab loop may be involved in sodium binding. For MtrF, Glu147 in repeat 1 and Asp449 in repeat 2 were found close to the regions that bind sodium in VcINDY and YdaH. Although the resolution of MtrF is low (3.95 Å), the structure refinement was performed with the aid of selenomethionine isomorphous replacement, and therefore the positioning of these ionizable residues close to the central pocket is likely to be accurate. Therefore, we propose that these two residues, Glu147 and Asp449, may be involved in interactions with a coupling ion, presumably protons. Finally, for YdaH, we predict that if transport involves more than one sodium ion, then residues Ser129, Ser130, Thr132, and Asp134 in HP1, and Ser167, Ser171, and Asn173 in TM3b and L3ab are the most likely candidates for forming an additional sodium-binding site, and that Asp134 is a reasonable candidate for proton binding.

Our structural analysis of MtrF, YdaH, and VcINDY led to the finding that the S[NHS]xx[ST]-related motifs in the hairpins, known already in INDY homologues of the DASS family, also extend to the drug transporters of the AbgT family. In VcINDY, residues in the HP1 motif contribute to the Na2 site, and our comparative analysis suggests that residues in the HP2 motif contribute to the Na3 site. Interestingly, however, the equivalent sequence motifs in the AbgT transporters are in slightly different positions structurally, and appear not to be involved in cation binding directly. Nevertheless, the conservation of these motifs in two distantly related families from a diverse superfamily suggests that small or polar residues are an important feature of the hairpin loops in this architecture, possibly for structural or other mechanistic reasons. The NaPi-II transporter family (TCDB 2.A.58), which probably shares a common core segment with VcINDY, but lacks four of the more peripheral TM segments, also contains two conserved QSS motifs that are predicted to be located in the equivalent hairpins; residues from these motifs abolish transport upon mutation (Fenollar-Ferrer et al., 2014). These observations suggest that the hairpin motifs are central to the mechanism of this apparently large class of transporters.

The relationship between the AbgT and DASS families within the umbrella of the ion transporter superfamily was inferred previously based on transitive homology involving two other families: AbgT to GntP (2.A.8), GntP to CitMHS (TCDB 2.A.11), and CitMHS to DASS (Prakash et al., 2003). This "daisy chain" establishes relationships even though direct comparisons between, for example YdaH (from the AbgT family) and VcINDY (from the DASS family) did not reveal any detectable sequence homology (Prakash et al., 2003). The observation that their structures have the same fold therefore strongly suggests that the GntP and CitMHS families also share this fold, and possibly others assigned to the ion transporter superfamily, such as the ArsB arsenite-antimonite efflux family (TCDB 2.A.45; Prakash et al., 2003).

Some of the largest differences between the three proteins occur in their dimerization domains. It is possible that such differences minimize the potential for heterodimer formation between unrelated but structurally similar transporters. However, because these three proteins are from different species, further analysis will be required to understand the roles of these differences (and their mechanistic implications) in native cellular physiology.

Our findings demonstrating a conserved fold among these proteins also have mechanistic implications. We speculate that even with divergence in detailed aspects of the mechanism, such as substrate specificity or antiport/symport, the nature of the conformational changes underlying transport are likely to be similar in scope among VcINDY, MtrF, and YdaH, and among the larger ion transporter superfamily. These structures provide little understanding about the basic mechanism of transport for these proteins, although their architectures, with clearly distinct transport and dimerization domains, suggest that they do not use the familiar "rocking bundle" conformational mechanism for alternating access. We have established here a fundamental architectural pattern among these proteins. Future work will be essential to define their precise mechanisms of transport and to understand the detailed features of their individual mechanisms, their commonalities, and their divergences.

REFERENCES

Bergeron, M.J., B. Clémençon, M.A. Hediger, and D. Markovich. 2013. SLC13 family of Na^+-coupled di- and tri-carboxylate/sulfate transporters. *Mol. Aspects Med.* 34:299–312. http://dx.doi.org/10.1016/j.mam.2012.12.001

Berman, H.M., J. Westbrook, Z. Feng, G. Gilliland, T.N. Bhat, H. Weissig, I.N. Shindyalov, and P.E. Bourne. 2000. The Protein Data Bank. *Nucleic Acids Res.* 28:235–242. http://dx.doi.org/10.1093/nar/28.1.235

Bolla, J.R., C.C. Su, J.A. Delmar, A. Radhakrishnan, N. Kumar, T.H. Chou, F. Long, K.R. Rajashankar, and E.W. Yu. 2015. Crystal structure of the *Alcanivorax borkumensis* YdaH transporter reveals an unusual topology. *Nat. Commun.* 6:6874. http://dx.doi.org/10.1038/ncomms7874

Boudker, O., R.M. Ryan, D. Yernool, K. Shimamoto, and E. Gouaux. 2007. Coupling substrate and ion binding to extracellular gate of a sodium-dependent aspartate transporter. *Nature.* 445:387–393. http://dx.doi.org/10.1038/nature05455

Chen, J.S., V. Reddy, J.H. Chen, M.A. Shlykov, W.H. Zheng, J. Cho, M.R. Yen, and M.H. Saier Jr. 2011. Phylogenetic characterization of transport protein superfamilies: Superiority of SuperfamilyTree programs over those based on multiple alignments. *J. Mol. Microbiol. Biotechnol.* 21:83–96. http://dx.doi.org/10.1159/000334611

Crisman, T.J., S. Qu, B.I. Kanner, and L.R. Forrest. 2009. Inward-facing conformation of glutamate transporters as revealed by their inverted-topology structural repeats. *Proc. Natl. Acad. Sci. USA.* 106:20752–20757. http://dx.doi.org/10.1073/pnas.0908570106

Crooks, G.E., G. Hon, J.M. Chandonia, and S.E. Brenner. 2004. WebLogo: A sequence logo generator. *Genome Res.* 14:1188–1190. http://dx.doi.org/10.1101/gr.849004

Edgar, R.C. 2010. Search and clustering orders of magnitude faster than BLAST. *Bioinformatics.* 26:2460–2461. http://dx.doi.org/10.1093/bioinformatics/btq461

Ehrnstorfer, I.A., E.R. Geertsma, E. Pardon, J. Steyaert, and R. Dutzler. 2014. Crystal structure of a SLC11 (NRAMP) transporter reveals the basis for transition-metal ion transport. *Nat. Struct. Mol. Biol.* 21:990–996. http://dx.doi.org/10.1038/nsmb.2904

Fang, Y., H. Jayaram, T. Shane, L. Kolmakova-Partensky, F. Wu, C. Williams, Y. Xiong, and C. Miller. 2009. Structure of a prokaryotic virtual proton pump at 3.2 Å resolution. *Nature.* 460:1040–1043.

Fenollar-Ferrer, C., M. Patti, T. Knöpfel, A. Werner, I.C. Forster, and L.R. Forrest. 2014. Structural fold and binding sites of the human Na^+-phosphate cotransporter NaPi-II. *Biophys. J.* 106:1268–1279. http://dx.doi.org/10.1016/j.bpj.2014.01.043

Finn, R.D., J. Clements, and S.R. Eddy. 2011. HMMER web server: interactive sequence similarity searching. *Nucleic Acids Res.* 39:W29–W37. http://dx.doi.org/10.1093/nar/gkr367

Folster, J.P., and W.M. Shafer. 2005. Regulation of *mtrF* expression in *Neisseria gonorrhoeae* and its role in high-level antimicrobial resistance. *J. Bacteriol.* 187:3713–3720. http://dx.doi.org/10.1128/JB.187.11.3713-3720.2005

Forrest, L.R. 2015. Structural symmetry in membrane proteins. *Annu Rev Biophys.* 44:311–337. http://dx.doi.org/10.1146/annurev-biophys-051013-023008

Forrest, L.R., Y.-W. Zhang, M.T. Jacobs, J. Gesmonde, L. Xie, B.H. Honig, and G. Rudnick. 2008. Mechanism for alternating access in neurotransmitter transporters. *Proc. Natl. Acad. Sci. USA.* 105:10338–10343. http://dx.doi.org/10.1073/pnas.0804659105

Forrest, L.R., R. Krämer, and C. Ziegler. 2011. The structural basis of secondary active transport mechanisms. *Biochim. Biophys. Acta.* 1807:167–188. http://dx.doi.org/10.1016/j.bbabio.2010.10.014

Forster, I., N. Hernando, J. Biber, and H. Murer. 1998. The voltage dependence of a cloned mammalian renal type II Na^+/P_i

cotransporter (NaP$_i$-2). *J. Gen. Physiol.* 112:1–18. http://dx.doi .org/10.1085/jgp.112.1.1

Forster, I.C., N. Hernando, J. Biber, and H. Murer. 2012. Phosphate transport kinetics and structure-function relationships of SLC34 and SLC20 proteins. *Curr. Top. Membr.* 70:313–356. http://dx .doi.org/10.1016/B978-0-12-394316-3.00010-7

Johnson, Z.L., C.G. Cheong, and S.Y. Lee. 2012. Crystal structure of a concentrative nucleoside transporter from *Vibrio cholerae* at 2.4Å. *Nature.* 483:489–493. http://dx.doi.org/10.1038/nature10882

Kabsch, W., and C. Sander. 1983. Dictionary of protein secondary structure: Pattern recognition of hydrogen-bonded and geo-metrical features. *Biopolymers.* 22:2577–2637. http://dx.doi.org/ 10.1002/bip.360221211

Katoh, K., and D.M. Standley. 2013. MAFFT multiple sequence alignment software version 7: Improvements in performance and usability. *Mol. Biol. Evol.* 30:772–780. http://dx.doi.org/10.1093/ molbev/mst010

Lomize, M.A., A.L. Lomize, I.D. Pogozheva, and H.I. Mosberg. 2006. OPM: Orientations of proteins in membranes data-base. *Bioinformatics.* 22:623–625. http://dx.doi.org/10.1093/ bioinformatics/btk023

Ma, D., P. Lu, C. Yan, C. Fan, P. Yin, J. Wang, and Y. Shi. 2012. Structure and mechanism of a glutamate-GABA antiporter. *Nature.* 483:632–636. http://dx.doi.org/10.1038/nature10917

Malinauskaite, L., M. Quick, L. Reinhard, J.A. Lyons, H. Yano, J.A. Javitch, and P. Nissen. 2014. A mechanism for intracellular re-lease of Na$^+$ by neurotransmitter/sodium symporters. *Nat. Struct. Mol. Biol.* 21:1006–1012. http://dx.doi.org/10.1038/nsmb.2894

Mancusso, R., G.G. Gregorio, Q. Liu, and D.N. Wang. 2012. Structure and mechanism of a bacterial sodium-dependent di-carboxylate transporter. *Nature.* 491:622–626. http://dx.doi.org/ 10.1038/nature11542

Mulligan, C., G.A. Fitzgerald, D.-N. Wang, and J.A. Mindell. 2014. Functional characterization of a Na$^+$-dependent dicarboxylate trans-porter from *Vibrio cholerae. J. Gen. Physiol.* 143:745–759. http:// dx.doi.org/10.1085/jgp.201311141

Pandit, S.B., and J. Skolnick. 2008. Fr-TM-align: a new protein structural alignment method based on fragment alignments and the TM-score. *BMC Bioinformatics.* 9:531. http://dx.doi.org/ 10.1186/1471-2105-9-531

Petřek, M., M. Otyepka, P. Banáš, P. Kosinová, J. Koca, and J. Damborský. 2006. CAVER: a new tool to explore routes from pro-tein clefts, pockets and cavities. *BMC Bioinformatics.* 7:316. http:// dx.doi.org/10.1186/1471-2105-7-316

Prakash, S., G. Cooper, S. Singhi, and M.H. Saier Jr. 2003. The ion transporter superfamily. *Biochim. Biophys. Acta.* 1618:79–92. http://dx.doi.org/10.1016/j.bbamem.2003.10.010

Ressl, S., A.C. Terwisscha van Scheltinga, C. Vonrhein, V. Ott, and C. Ziegler. 2009. Molecular basis of transport and regulation in the Na$^+$/betaine symporter BetP. *Nature.* 458:47–52. http:// dx.doi.org/10.1038/nature07819

Reyes, N., C. Ginter, and O. Boudker. 2009. Transport mechanism of a bacterial homologue of glutamate transporters. *Nature.* 462:880–885. http://dx.doi.org/10.1038/nature08616

Saier, M.H., Jr., C.V. Tran, and R.D. Barabote. 2006. TCDB: the transporter classification database for membrane transport pro-tein analyses and information. *Nucleic Acids Res.* 34:D181–D186. http://dx.doi.org/10.1093/nar/gkj001

Shaffer, P.L., A. Goehring, A. Shankaranarayanan, and E. Gouaux. 2009. Structure and mechanism of a Na$^+$-independent amino acid transporter. *Science.* 325:1010–1014. http://dx.doi.org/10.1126/ science.1176088

Stamm, M., and L.R. Forrest. 2015. Structure alignment of mem-brane proteins: Accuracy of available tools and a consensus strategy. *Proteins.* 83:1720–1732. http://dx.doi.org/10.1002/prot .24857

Su, C.C., J.R. Bolla, N. Kumar, A. Radhakrishnan, F. Long, J.A. Delmar, T.H. Chou, K.R. Rajashankar, W.M. Shafer, and E.W. Yu. 2015. Structure and function of *Neisseria gonorrhoeae* MtrF illumi-nates a class of antimetabolite efflux pumps. *Cell Reports.* 11:61–70. http://dx.doi.org/10.1016/j.celrep.2015.03.003

Watanabe, A., S. Choe, V. Chaptal, J.M. Rosenberg, E.M. Wright, M. Grabe, and J. Abramson. 2010. The mechanism of sodium and substrate release from the binding pocket of vSGLT. *Nature.* 468:988–991. http://dx.doi.org/10.1038/nature09580

Waterhouse, A.M., J.B. Procter, D.M. Martin, M. Clamp, and G.J. Barton. 2009. Jalview Version 2—a multiple sequence alignment editor and analysis workbench. *Bioinformatics.* 25:1189–1191. http://dx.doi.org/10.1093/bioinformatics/btp033

Weyand, S., T. Shimamura, S. Yajima, S. Suzuki, O. Mirza, K. Krusong, E.P. Carpenter, N.G. Rutherford, J.M. Hadden, J. O'Reilly, et al. 2008. Structure and molecular mechanism of a nucleobase-cation-symport-1 family transporter. *Science.* 322:709–713. http://dx.doi.org/10.1126/science.1164440

Yamashita, A., S.K. Singh, T. Kawate, Y. Jin, and E. Gouaux. 2005. Crystal structure of a bacterial homologue of Na$^+$/Cl$^-$-dependent neurotransmitter transporters. *Nature.* 437:215–223. http://dx .doi.org/10.1038/nature03978

Yernool, D., O. Boudker, Y. Jin, and E. Gouaux. 2004. Structure of a glutamate transporter homologue from *Pyrococcus horikoshii. Nature.* 431:811–818. http://dx.doi.org/10.1038/nature03018

Zhang, Y., and J. Skolnick. 2004. Scoring function for automated assessment of protein structure template quality. *Proteins.* 57:702–710. http://dx.doi.org/10.1002/prot.20264